CrystEngComm

RSC Publishing

PAPER

View Article Online
View Journal | View Issue

Cite this: *CrystEngComm*, 2013, **15**, 3593

Chirality and absolute helicity in a pair of enantiomeric amino acid derivatives and their complexes: structures, chiroptical, and photoluminescent properties†

Xinfa Li,* Huajun Zhao and Qihua Zeng

Received 15th December 2012,
Accepted 6th February 2013

DOI: 10.1039/c3ce27028a

www.rsc.org/crystengcomm

A pair of enantiomeric amino acid derivatives [L-H_2cala (**1L**) and D-H_2cala (**1D**), H_2cala = *N*-(4-carboxylbenzyl)-alanine] were synthesized by a one step substitution reaction of enantiopure L-(or D-)alanine with 4-(bromomethyl)benzoic acid. Self-assembly of **1L** and **1D** with divalent Cu^{2+} and Cd^{2+} ions in water produced two pairs of enantiomers formulated as $[Cu(L\text{-cala})(H_2O)]_n{\cdot}n(H_2O)$ (**2L**), $[Cu(D\text{-cala})(H_2O)]_n{\cdot}n(H_2O)$ (**2D**), $[Cd(L\text{-Hcala})_2(H_2O)_2]_n{\cdot}n(H_2O)$ (**3L**) and $[Cd(D\text{-Hcala})_2(H_2O)_2]_n{\cdot}n(H_2O)$ (**3D**). X-ray diffraction analyses reveal that **1L** and **1D** are hydrogen-bonded two-dimensional (2D) supramolecules containing one-dimensional (1D) single-stranded supramolecular helices parallel to the crystallographic *b*-axis. **2L** and **2D** are 1D single-stranded coordination helices arranged along the direction of *c*-axis. They are further extended into three-dimensional (3D) supramolecular frameworks by inter-helical hydrogen bonds. **3L** and **3D** are 1D single-stranded coordination helices parallel to *a*-axis. Then three neighboring single-stranded coordination helices are further tied up by hydrogen bonds, forming 1D triple-stranded supramolecular helices extending along the same direction. Interestingly, **3L** and **3D** also show supramolecular helicities on the directions of *b*- and *c*-axes. The chiralities and absolute helicities of these complexes are controlled by the chiralities of ligands. In addition, the solid-state circular dichroism (CD) and photoluminescent properties of them were investigated.

Introduction

Chirality and helicity are prevalent in living and nonliving systems at the molecular and supramolecular levels.[1] However, the relationship between chirality of molecular building units and absolute helicity of polymeric structures is still unclear, even if it is known unambiguously that the absolute helicity of α-helices in the secondary structures of two most important biopolymers (natural protein and DNA) are right-handed.[2] This is also intimately related to the origin of asymmetry in the biological process where proteins are exclusively composed of L-(α)-amino acids while DNAs are merely made of D-sugars.[3]

Natural amino acids are uniformly the L-form (except the optically inactive glycine) as a result of the chirality on the α-C. The α-helices of proteins are typically single-stranded and appear in a right-handed conformation due to the selective incorporation of L-amino acids.[2] The driven force in the formation of α-helices is hydrogen bonds between amino and carbonyl groups of L-amino acids. Complexes constructed from L-amino acid ligands appear in left-handed (*M*) conformation more than in right-handed (*P*) conformation, where the main driving forces are coordination bonds between L-amino acid ligands and metal ions.[4–10] On the contrary, α-helices composed of D-amino acids display *M* conformation and complexes containing D-amino acid ligands prefer *P* conformation to *M* conformation. This is also the situation for ligands derived from amino acids.[11–19] Schiff base and reduced Schiff base synthesized by the condensation of amino acids and salicylaldehyde or pyridinecarboxaldehyde are the most popular ligands of this kind. One of the most interesting examples is a 1D left-handed helical coordination polymer $[(H_2O)_2@\{Ni(L\text{-Hsglu})(H_2O)_2\}]{\cdot}H_2O$ [L-H_3sglu = *N*-(2-hydroxybenzyl)-L-glutamic acid] encapsulating a 1D left-handed water helix in each of its channels.[13a] More recently, two 1D helical structures $[Cu(L\text{-pasp})(H_2O)]{\cdot}4H_2O$ (a infinite single-stranded *M*-helix) and $[Cu(D\text{-pasp})(H_2O)]{\cdot}4H_2O$ (an infinite single-stranded *P*-helix) [H_2pasp = *N*-(2-pyridylmethyl)-aspartic acid],[14] and two enantiomeric lanthanide clusters $[La_7\{(S)\text{-}L\}_6(CO_3)(NO_3)_6(OCH_3)(CH_3OH)_7]{\cdot}2CH_3OH{\cdot}5H_2O$ (a finite triple-stranded *M*-helix) [(*S*)-H_2L = *N*-(2-hydroxybenzyl)-L-asparagine] and $[La_7\{(R)\text{-}L\}_6(CO_3)(NO_3)_6(OCH_3)(CH_3OH)_7]{\cdot}2CH_3OH{\cdot}5H_2O$ (a finite triple-stranded *P*-helix) [(*R*)-H_2L = *N*-(2-hydroxybenzyl)-D-asparagine] were reported.[15] It is noteworthy that the intrinsic chirality of amino acid ligands that originated

Department of Chemistry, Zunyi Normal College, Zunyi, 563002, P. R. China. E-mail: xflichem@163.com

† Electronic supplementary information (ESI) available: Crystallographic file for **1L** to **3D** in CIF format; Fig. S1–S15 and Table S1. CCDC 916191–916194. For ESI and crystallographic data in CIF or other electronic format see DOI: 10.1039/c3ce27028a

from the α-C have been transferred into these crystal structures, and the relationship between ligand chirality and absolute helicity is in accordance with the above-mentioned principle. However, the principle is not absolute, and the coordination configuration preference of metal ions also affects the absolute helicity of coordination polymers, in which the mechanism of chirality transfer from ligand to complexes and crystals is rather complicated and unexpectable.[18–20]

Herein we report three pairs of enantiomeric coordination helices and supramolecular helices based on *N*-(4-carboxylbenzyl)-L(or D)-alanine ligands: L-H_2cala (**1L**) and D-H_2cala (**1D**), $[Cu(L\text{-cala})(H_2O)]_n \cdot n(H_2O)$ (**2L**) and $[Cu(D\text{-cala})(H_2O)]_n \cdot n(H_2O)$ (**2D**), $[Cd(L\text{-Hcala})_2(H_2O)_2]_n \cdot n(H_2O)$ (**3L**) and $[Cd(D\text{-Hcala})_2(H_2O)_2]_n \cdot n(H_2O)$ (**3D**), concerning their syntheses, crystal structures, chiroptical, and photoluminescent properties. H_2cala ligands have an aromatic and an aliphatic carboxyl group on two opposite orientations with both rigidity and flexibility, making them prone to form helical structures when coordinating to metal ions. These compounds may provide fresh models for studying the relationship between molecular chirality and supramolecular absolute helicity in biopolymers.

Experimental

Materials and general methods

All chemicals were obtained from commercial sources and used without further purification. Infrared (IR) spectra were recorded on PerkinElmer Spectrum One instrument as KBr pellets in the range of 4000–400 cm^{-1}. Elemental analyses of C, H and N were measured on a Vario MICRO E III elemental analyzer. The ^{1}H-NMR spectra of **1L** ligand was recorded on a BRUKER AVANCE III-400M NMR spectrometer in deuterated d_6-DMSO. Powder XRD patterns were collected on a Rigaku Mini Flex II diffractometer using Cu Kα Radiation (λ = 1.54056 Å) under ambient conditions. Thermogravimetric analyses were performed on an SDT Q600 instrument at a heating rate of 10 °C min^{-1} under a nitrogen atmosphere. Solid-state photoluminescent spectra of **1L** and **3L** were measured at room temperature with an Edinburgh FLS920 fluorescence spectrometer. The instrument is equipped with a Xe900 xenon arc lamp as exciting light source. Solid-state CD spectra of **1L**–**3D** were recorded using a BioLogic-MOS 450 spectrometer at room temperature. For each CD measurement *ca.* 0.5 mg crystalline sample was taken to be mixed with 100 mg of dried and well ground KCl powder. This mixture was then pressed into a disk by a literature method.[11]

Syntheses of L-H_2cala (1L) and D-H_2cala (1D) ligands. Although the synthesis of **1L** was previously published,[21] herein we report a different but more productive method. Enantiopure L-alanine (for **1L** or D-alanine for **1D**) (50 mmol) and NaOH (60 mmol) were dissolved in 40 mL distilled water and magnetically stirred at room temperature, to which 4-(bromomethyl)benzoic acid (10 mmol) was added in small portions. The mixture was stirred for about 1.5 h and then heated to reflux on an oil bath for about 40 min. After cooling to room temperature, 6 M HCl was added dropwise to a pH value of about 4.0. Large amounts of white precipitate thus formed was collected by vacuum filtration, followed by washing repeatedly with distilled water and then with EtOH. The product was finally dried in a vacuum desiccator equipped with allochroic silica gel. Yield: 67% [based on 4-(bromomethyl)benzoic acid]. The yield is significantly higher than that of the method reported in the literature (45%).[21] Calculated for $C_{11}H_{13}NO_4$ (%): C, 59.19; H, 5.87; N, 6.27. Found for **1L** (%): C, 59.11; H, 5.90; N, 6.22. Found for **1D** (%): C, 59.15; H, 5.88; N, 6.25. IR (KBr pellet, cm^{-1}): 3414 (br), 3035 (m), 2450–2700 (br, w), 1705 (s), 1615 (vs), 1452 (w), 1398 (m), 1346 (w), 1258 (s), 1118 (w). ^{1}H-NMR in deuterated DMSO (ppm): 7.92 (d, H3 and H7), 7.51 (d, H4 and H6), 3.98 (d, H8A), 3.87 (d, H8B), 3.17 (q, H10), 1.24 (d, H11A, H11B and H11C). It should be noted that H8A and H8B are chemically inequivalent due to the steric hindrance of the large $-C_6H_4CO_2H$ group, so their chemical shifts are split into two adjacent peaks in the NMR spectrum. An X-ray quality single crystal of **1L** was obtained by recrystallization in H_2O.

Syntheses of $[Cu(L\text{-cala})(H_2O)]_n \cdot n(H_2O)$ (2L) and $[Cu(D\text{-cala})(H_2O)]_n \cdot n(H_2O)$ (2D). $Cu(CH_3CO_2)_2 \cdot H_2O$ (0.4 mmol) was dissolved in 5 mL hot water and magnetically stirred, to which L-H_2cala (for **2L** or D-H_2cala for **2D**) (0.4 mmol) was added. A dark blue clear solution appeared immediately, which was filtered 10 min later. The filtrate was sealed and placed in an oven at 50 °C for about 24 h. Large prism-shaped dark blue crystals were harvested. The crystals were collected by filtration and air-dried. Yield: 80% (based on $Cu(CH_3CO_2)_2 \cdot H_2O$). Calculated for $C_{11}H_{15}CuNO_6$ (%): C, 41.19; H, 4.71; N, 4.37. Found for **2L** (%): C, 41.15; H, 4.75; N, 4.39. Found for **2D** (%): C, 41.14; H, 4.77; N, 4.36. IR (KBr pellet, cm^{-1}): 3501 (br), 3148 (m), 1610 (vs), 1558 (m), 1452 (w), 1375 (s), 1092 (w).

Syntheses of $[Cd(L\text{-Hcala})_2(H_2O)_2]_n \cdot n(H_2O)$ (3L) and $[Cd(D\text{-Hcala})_2(H_2O)_2]_n \cdot n(H_2O)$ (3D). L-H_2cala (for **3L** or D-H_2cala for **3D**) (0.4 mmol) and NaOH (0.4 mmol) were dissolved in 6 mL distilled water, to which $Cd(NO_3)_2 \cdot 4H_2O$ (0.2 mmol) was added. The colorless clear solution thus obtained was filtered and placed undisturbed at room temperature for 48 h. Colorless small needle crystals were collected by filtration and air-dried. Yield: 82% (based on $Cd(NO_3)_2 \cdot 4H_2O$). Calculated for $C_{22}H_{30}CdN_2O_{11}$ (%): C, 43.25; H, 4.95; N, 4.59. Found for **3L** (%): C, 43.18; H, 4.97; N, 4.55. Found for **3D** (%): C, 43.22; H, 4.91; N, 4.58. IR (KBr pellet, cm^{-1}): 3434 (br), 3054 (w), 2450–2700 (br, w), 1600 (vs), 1542 (m), 1464 (w), 1396 (s), 1362 (s), 1106 (w).

X-ray crystallographic studies

Crystal structure determinations for **1L**, **2D** and **3L** were performed on an Oxford Xcalibur E CCD-based diffractometer equipped with graphite-monochromated Mo Kα radiation (λ = 0.71073 Å) at room temperature. The intensity data sets were collected with the ω-scan technique. The CrysAlisPro (Version 1.171.34.49) software was used for data reduction and empirical absorption correction. Crystal structure determination of **2L** was performed on a Rigaku SCX-mini CCD-based diffractometer equipped with graphite-monochromated Mo

Table 1 Crystallographic data for **1L**, **2L**, **2D** and **3L**

	1L	**3L**
[a] $R = \Sigma\|\|F_o\| - \|F_c\|\|/\Sigma\|F_o\|$, $wR = [\Sigma w(F_o^2 - F_c^2)^2/\Sigma w(F_o^2)^2]^{1/2}$.		
Empirical formula	$C_{11}H_{13}NO_4$	$C_{22}H_{30}CdN_2O_{11}$
Formula weight	223.22	610.88
Crystal system	Monoclinic	Orthorhombic
Space group	$P2_1$	$P2_12_12_1$
a/Å	7.3335(6)	5.8266(2)
b/Å	5.8827(4)	17.2093(7)
c/Å	12.8465(9)	23.5764(1)
β/°	99.790(7)	90
V/Å^3	546.14(7)	2364.05(16)
Z	2	4
D_c/g cm^{-3}	1.357	1.716
μ/mm^{-1}	0.104	0.990
R_{int}	0.0180	0.0326
Data/parameters	1533/146	4174/327
Flack x	0.4(14)	−0.04(3)
GOF on F^2	1.012	1.001
R_1, wR_2 ($I > 2\sigma(I)$)[a]	0.0337, 0.0585	0.0378, 0.0763
R_1, wR_2 (all data)[a]	0.0508, 0.0606	0.0593, 0.0840
$\Delta\rho_{min/max}$ [e Å^{-3}]	0.120/−0.147	0.446/−0.432
	2L	**2D**
Empirical formula	$C_{11}H_{15}CuNO_6$	$C_{11}H_{15}CuNO_6$
Formula weight	320.78	320.78
Crystal system	Tetragonal	Tetragonal
Space group	$P4_3$	$P4_1$
$a = b$/Å	7.5402(2)	7.5385(1)
c/Å	22.7232(1)	22.7308(1)
V/Å^3	1291.92(7)	1291.77(7)
Z	4	4
D_c/g cm^{-3}	1.649	1.649
μ/mm^{-1}	1.712	1.713
R_{int}	0.0401	0.0264
Data/parameters	2847/173	1851/173
Flack x	−0.004(16)	0.009(16)
GOF on F^2	1.008	1.004
R_1, wR_2 ($I > 2\sigma(I)$)[a]	0.0356, 0.0832	0.0298, 0.0632
R_1, wR_2 (all data)[a]	0.0370, 0.0845	0.0330, 0.0649
$\Delta\rho_{min/max}$ [e Å^{-3}]	0.269/−0.514	0.323/−0.281

Kα radiation (λ = 0.71073 Å) at room temperature. The CrystalClear software was used for data reduction and empirical absorption correction. All the structures were solved by direct methods and successive Fourier difference syntheses, and refined by full-matrix least-squares on F^2 (SHELXL Version 5.1).[22] All non-hydrogen atoms were refined with anisotropic displacement parameters. Hydrogen atoms attached to C, N and protonated carboxyl O atoms were generated theoretically and refined by a riding-mode with isotropic thermal parameters fixed at 1.2 times that of the mother atoms. Positions of hydrogen atoms bonding to water molecules were calculated by the PLATON program,[23] and then refined in the SHELXL program with isotropic thermal parameters fixed at 1.5 times that of the corresponding O atoms. Detailed crystallographic data and structure refinement parameters of **1L**, **2L**, **2D** and **3L** are summarized in Table 1. Selected bond lengths are listed in Table 2. Hydrogen-bonding parameters are listed in Table S1 (ESI†).

Table 2 Selected bond lengths [Å] for **1L**, **2L**, **2D** and **3L**[a]

1L			
[a] Symmetry codes: for **2L** #1 $y + 1$, $-x + 1$, $z + 1/4$. For **3L** #1 $x - 3/2$, $-y + 1/2$, $-z + 2$.			
O(1)–C(1)	1.311(3)	O(2)–C(1)	1.199(3)
O(3)–C(9)	1.262(3)	O(4)–C(9)	1.241(3)
2L			
Cu(1)–O(3)	1.919(2)	Cu(1)–O(5)	1.922(3)
Cu(1)–O(1)	1.950(3)	Cu(1)–N(1)#1	2.011(3)
2D			
Cu(1)–O(5)	1.922(3)	Cu(1)–O(3)	1.923(2)
Cu(1)–O(1)	1.949(3)	Cu(1)–N(1)	2.017(3)
3L			
Cd(1)–O(9)	2.258(4)	Cd(1)–O(10)	2.269(4)
Cd(1)–O(5)	2.272(4)	Cd(1)–O(4)#1	2.315(4)
Cd(1)–O(1)	2.327(4)	Cd(1)–O(2)	2.556(4)
Cd(1)–O(6)	2.668(5)		

Results and discussion

Crystal structures of L-H_2cala (1L) and D-H_2cala (1D)

As shown in Scheme 1, L-H_2cala (**1L**) and D-H_2cala (**1D**) are one pair of enantiomers. They have the same structure except the opposite chirality on C(10), which stems from amino acids used in the synthetic process (enantiopure L-alanine for **1L** and D-alanine for **1D**). So **1L** is taken as representative to depict their structures. Single crystal X-ray diffraction analysis reveals that **1L** crystallizes in the chiral $P2_1$ space group (no. 4). Due to the lack of atoms heavier than Si in **1L**, the absolute structure cannot be determined by the anomalous dispersion effects in diffraction measurements on the crystal.[24] However, the synthetic process does not change the chirality on C(10), so the absolute configuration is predetermined to be the L-form. As displayed in Fig. 1, the asymmetric unit of **1L** is composed of a zwitterionic L-H_2cala molecule. It is interesting that the deprotonated carboxyl group is C(9)O_2H rather than C(1)O_2H, as suggested by C–O bonding parameters [the C(1)–O(1), C(1)–O(2), C(9)–O(3) and C(9)–O(4) bond lengths are 1.311(3), 1.199(3), 1.262(3) and 1.241(3) Å, respectively (Table 2)]. It is obvious that C(1)–O(1) is a single bond, C(1)–O(2) is a double bond, while C(9)–O(3) and C(9)–O(4) are partially delocalized bonds lying between single and double bonds. Further evidence of the presence of both protonated and deprotonated carboxyl groups can also be found in the IR spectrum [Fig. S1(a) (ESI†) 1705 cm^{-1} ($\nu_{as}CO_2H$,), 1615 cm^{-1} ($\nu_{as}CO_2^-$)]. The amino group [N(1)H_2] is protonated to form two charge-assisted intermolecular hydrogen bonds with O atoms [O(3)

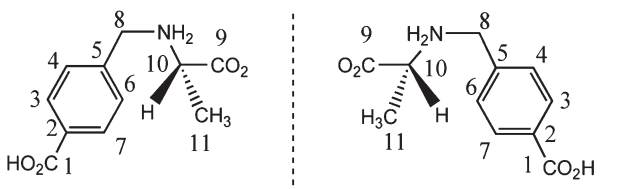

Scheme 1 Schematic drawing of L-H_2cala (left) and its mirror image D-H_2cala (right).

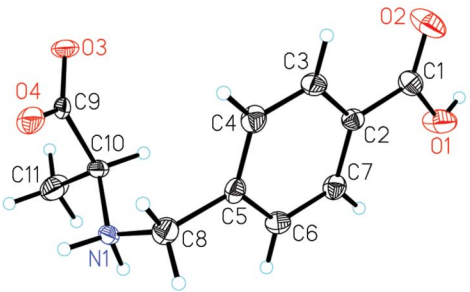

Fig. 1 ORTEP drawing of **1L** with 30% probability of thermal ellipsoids.

and O(4)] from adjacent L-H_2cala molecules [$^+$N(1)–H(1B)···O(3) (x, y − 1, z) with a D···A distance of 2.759(3) Å and $^+$N(1)–H(1C)···O(4) (−x, y − 1/2, −z + 1) with a D···A distance of 2.783(3) Å]. As presented in Fig. 2, the protonated carboxyl group acts as a hydrogen bond donor [O(1)–H(1A)···O(3) (−x + 1,y − 1/2,−z + 2) with a D···A distance of 2.593(2) Å)] which facilitates the formation of a 1D supramolecular helix along with another hydrogen bond [$^+$N(1)–H(1B)···O(3) (x, y − 1, z)]. The single-stranded supramolecular helix has right-handed absolute helicity, consistent with that of α-helices in natural proteins composed of L-amino acids. It is not strange since the formation of helix in **1L** is driven exclusively by hydrogen bonds, just like the secondary structure in natural proteins. The *P*-helix is arranged parallel to the *b*-axis with a 2_1 screw axis and a pitch of 5.8827 Å (equal to a length of unit cell parameter *b*). Viewed along the direction of the *b*-axis, the inner sphere of the helix is a tubular channel surrounded by two L-H_2cala molecules (Fig. S2, ESI†). The shortest separation between two parallel neighboring phenyl rings within the tube is about 5.883 Å (based on the centers of the two parallel phenyl rings), implying no π–π stacking interaction between

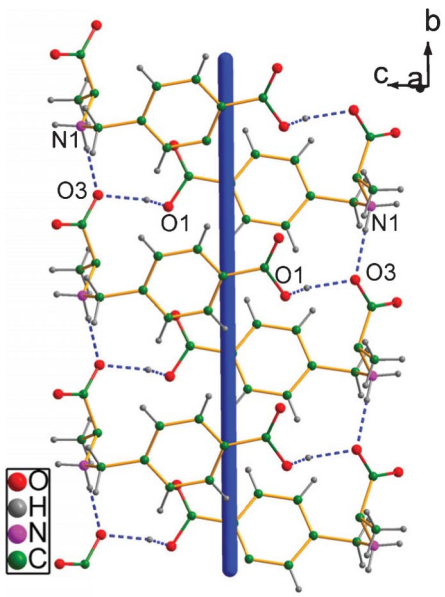

Fig. 2 The 1D supramolecular *P*-helix in **1L**.

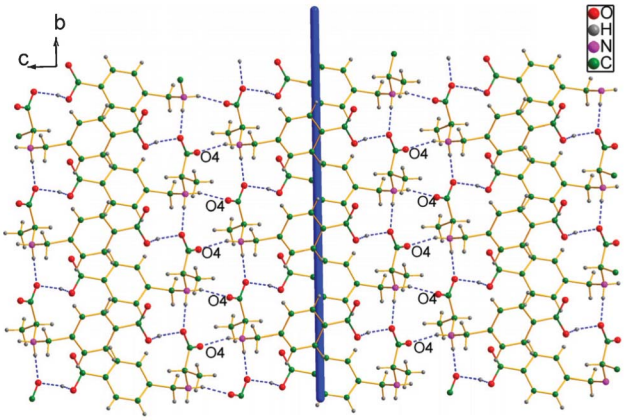

Fig. 3 View of the 2D supramolecular network of **1L** along *a*-axis.

them. Adjacent helices are further connected to each other by a charge-assisted hydrogen bond $^+$N(1)–H(1C)···O(4) (−x, y − 1/2, −z + 1) along the *c*-axis, generating a 2D supramolecular layer in the *bc*-plane (Fig. 3). Neighboring layers are packed to one another by van der Waals' interactions and there are no interlayer hydrogen bonds and π–π interactions. The supramolecular structure of **1D** is identical to **1L**, besides **1D** is just a single-stranded *M*-helix. A simulated comparison of the absolute helicities of **1L** and **1D** along the direction of the *b*-axis is displayed in Fig. S3 (ESI†).

It should be noted that the conformation relating to C(8) and N(1) is a *gauche*-form with the two larger –$CH(CH_3)CO_2^-$ and –$C_6H_4CO_2H$ groups lying adjacent to each other [Fig. S4(a), ESI†], distinct from the staggered conformation observed in a comparable *N*-(2-pyridylmethyl)-L-alanine zwitterion reported by us recently.[11] It is speculated that the relatively less stable *gauche* conformation in L-H_2cala may be advantageous to the formation of stronger intermolecular hydrogen bonds, which may also explain the chemical inequivalence of H8A and H8B in the NMR spectrum.

Crystal structures of [Cu(L-cala)(H_2O)]$_n$·n(H_2O) (2L) and [Cu(D-cala)(H_2O)]$_n$·n(H_2O) (2D)

Single crystal X-ray diffraction analyses demonstrate that **2L** and **2D** crystallize in the chiral $P4_3$ (no. 78) and $P4_1$ (no. 76) space groups, respectively. It means that they are also a pair of enantiomers, which is further confirmed by CD spectra. $P4_3$ and $P4_1$ are enantiomorphic space groups of each other (the enantiomorph of 4_3 screw axis is 4_1 screw axis). If one is a *M*-helix, the other should be a *P*-helix. **2L** and **2D** have the same unit cell parameters (with a deviation lower than 0.033%) and powder XRD patterns [Fig. S5(a), ESI†]. As shown in Fig. 4, the asymmetric unit of **2L** consists of one Cu^{2+} ion, a L-$cala^{2-}$ anion, an aqua ligand and one lattice H_2O molecule. L-$Cala^{2-}$ anion acts as a tridentate ligand by chelating to one Cu^{2+} bidentately *via* the amino N atom and the aliphatic carboxyl O atom to form a five-membered ring [–$CuOC_2N$–] and simultaneously coordinating to an equivalent Cu^{2+} ion monodentately through the aromatic carboxyl group (Fig. S6, ESI†). Cu^{2+} ion adopts a distorted square coordination geometry with a [NO_3] donor set. The *trans* position of the N

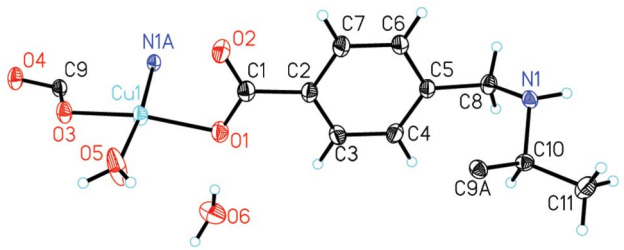

Fig. 4 ORTEP drawing of **2L** with 30% probability of thermal ellipsoids.

atom is an aqua ligand, and the other two coordination sites are taken up by two carboxyl O atoms. However, the five [$CuNO_3$] atoms are not coplanar, indicating the square is distorted. The Cu–N and Cu–O bond lengths are 2.011(3), 1.919(2), 1.922(3) and 1.950(3) Å, respectively (Table 2). The interconnection between Cu^{2+} and L-$cala^{2-}$ results in the formation of a 1D single-stranded coordination helix propagating along the crystallographic *c*-axis. The fourfold helix, with a pitch of 22.7232 Å (equal to length of unit cell *c*), is left-handed and symmetry-related by a 4_3 screw axis (Fig. 5). It differs from the absolute helicity of α-helices in natural proteins composed of L-amino acids. The difference originates from the mode how the chirality of α-C in L-amino acids influences the orientation of helices. α-Helices in proteins are formed exclusively by hydrogen bonds between amino and carbonyl groups. The orientation of α-helices is dependent on the steric hindrance effects between side-chain groups and main-chain moieties in proteins, which energetically prefers the right-handed conformation. Here the orientation of [Cu(L-cala)$(H_2O)]_n$ coordination helix is directly determined by the direction of the side-chain $-CH_2C_6H_4CO_2^-$ group, which is

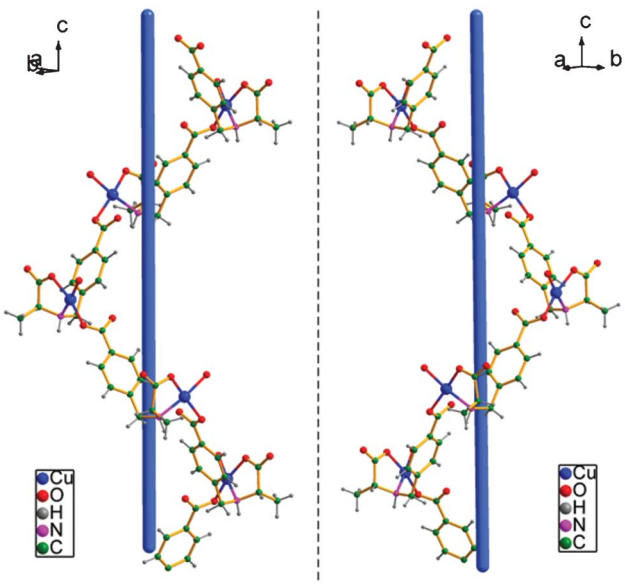

Fig. 5 The absolute helicities of **2L** (left) and its enantiomer **2D** (right) on the direction of *c*-axis. The mirror is drawn as a dash line. **2L** is a single-stranded *M*-helix and **2D** is a single-stranded *P*-helix.

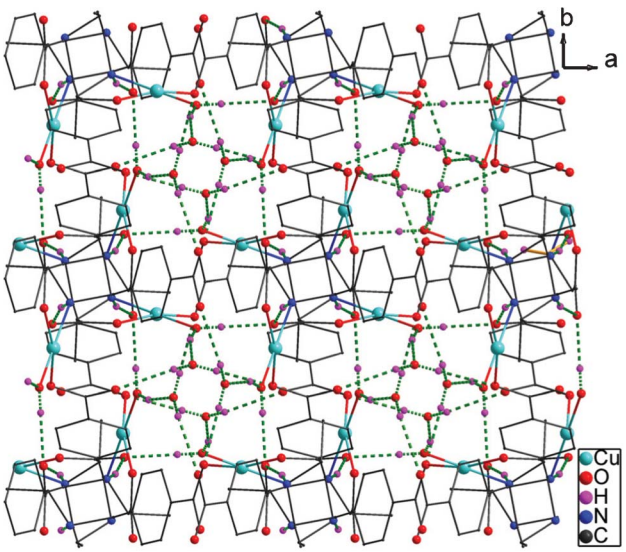

Fig. 6 View of the 3D supramolecular framework of **2L** along *c*-axis.

controlled by the chirality of L-$cala^{2-}$ ligand. Extensive hydrogen-bonding associations exist between L-$cala^{2-}$ ligands and H_2O molecules, which further joins adjacent helices together to form a 3D supramolecular framework (Fig. 6 and S7, ESI†). The crystal structure of **2D** is the same as **2L**, except that **2D** is a *P*-helix with a 4_1 screw axis parallel to the *c*-axis, suggesting they are mirror images of each other (Fig. 5). The Flack *x* parameters of **2L** and **2D** are −0.004 and 0.009, respectively (Table 1), indicative of the right absolute structures determined by the anomalous dispersion effects during diffraction data collection.[24,25]

The most interesting aspect in the structure of **2L** and **2D** is that the H_2cala ligand contains a cryptochiral N(1) atom. The deprotonation and following coordination to Cu^{2+} ion bring about two new chiral centers [N(1) and Cu(1)]. The generation of chirality on Cu(1) is also benefited from the distortion of the [$CuNO_3$] coordination square.[26] $S_{C(10)}$ (L-$cala^{2-}$) leads to $R_{N(1)}$, $\Lambda_{Cu(1)}$ and *M*-helix in **2L**, while $R_{C(10)}$ (D-$cala^{2-}$) gives rise to the opposite $S_{N(1)}$, $\Lambda_{Cu(1)}$ and *P*-helix in **2D** (Fig. S8, ESI†). Obviously, the absolute configuration of C(10) is predetermined and unchangeable, but those of N(1), Cu(1) and the absolute helicity of the coordination helix are cryptical and variable. It is reasonable to say that the chiralities on N(1), Cu(1) and the helices are dependent on that of C(10), namely, the self-assembly and crystallization process are highly stereoselective. In other words, the chirality transfer from ligand to complex and crystal is efficient. Similar to the case in **1L**, the conformation relating to C(8) and N(1) in **2L** and **2D** is also the relatively less stable *gauche*-form [Fig. S4(b), ESI†].

Crystal structures of $[Cd(L\text{-}Hcala)_2(H_2O)_2]_n \cdot n(H_2O)$ (3L) and $[Cd(D\text{-}Hcala)_2(H_2O)_2]_n \cdot n(H_2O)$ (3D)

X-ray diffraction analyses, CD, elemental analyses (EA) and IR spectra demonstrate that **3L** and **3D** are also a pair of enantiomers with the same chemical formulae. According to single crystal X-ray diffraction, **3L** crystallizes in the chiral

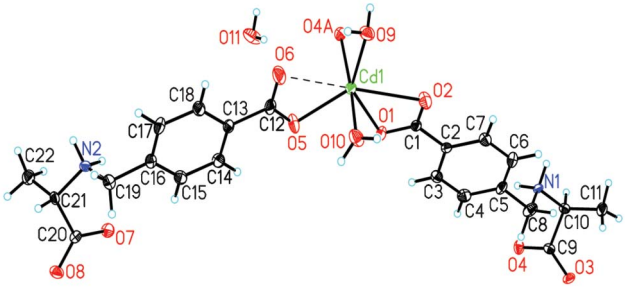

Fig. 7 ORTEP drawing of **3L** with 30% probability of thermal ellipsoids.

$P2_12_12_1$ (no. 19) space group with a Flack *x* parameter of −0.04 (Table 1), indicating the right absolute structure.[24,25] As shown in Fig. 7, the asymmetric unit of **3L** is composed of a Cd^{2+} ion, two L-Hcala$^-$ anions, two aqua ligands and one lattice H_2O molecule. Cd^{2+} adopts a slightly distorted pentagonal bipyramid coordination geometry with a [O_7] donor set (Fig. S9, ESI†). The five coordination sites on the equatorial plane are occupied by one H_2O molecule and four carboxyl O atoms from two crystallographically unique L-Hcala$^-$ ligands. The axial positions are taken up by one H_2O molecule and one carboxyl O atom from L-Hcala$^-$ ligand. The Cd–O bond lengths range from 2.258(4) to 2.668(5) Å, with an average value of about 2.381 Å (Table 2). L-Hcala$^-$ ligands exhibit two different coordination modes (Fig. S10, ESI†): (a) terminal mode: chelates to a Cd^{2+} bidentately *via* the aromatic carboxyl group; (b) bridging mode: chelates to a Cd^{2+} bidentately *via* the aromatic carboxyl group and again bridges to an equivalent Cd^{2+} ion monodentately through the aliphatic carboxyl group. All of the four carboxyl groups are deprotonated. Both of the amino groups [N(1)H_2 and N(2)H_2] are protonated as hydrogen bond donors and for charge-balance. The interlinkage between Cd^{2+} ion and the bridging L-Hcala$^-$ ligand leads to the formation of a 1D single-stranded coordination helix as shown in Fig. 8(a). The twofold helix is arranged parallel to the *a*-axis with a 2_1 screw axis and a pitch of 17.4798 Å (three times of the length of unit cell *a*). The absolute helicity of the helix is also left-handed, consistent with that in **2L** since both of them are formed by coordination bonds rather than hydrogen bonds. The terminal L-Hcala$^-$ ligand points to the direction of the *c*-axis, engaging in hydrogen-bonding formation. It is particularly interesting that three independent single-stranded coordination helices are joined together by hydrogen bonds, giving rise to a 1D triple-stranded supramolecular *M*-helix with a pitch of 5.8266 Å (equal to length of unit cell *a* and one-third of the pitch of a single-stranded coordination helix) (Fig. 8). The triple-stranded supramolecular helix is also symmetry-related by a 2_1 screw axis parallel to *a*-axis.

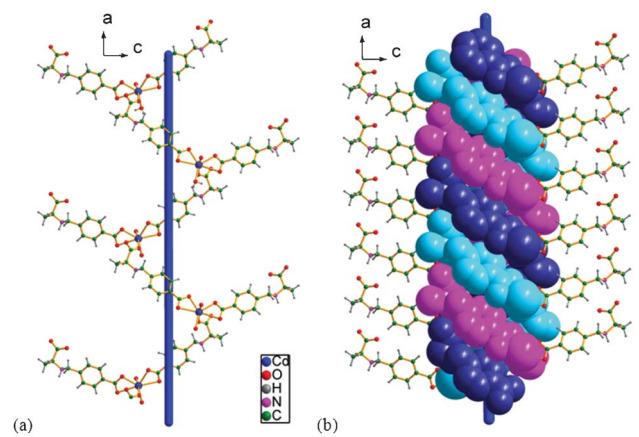

Fig. 8 Absolute helicity of **3L** on the direction of *a*-axis. (a) A single-stranded coordination polymeric *M*-helix. (b) A triple-stranded supramolecular *M*-helix.

On the direction of *b*-axis, the bridging L-Hcala$^-$ ligand is extended in a head-and-tail way by hydrogen bonds involving the lattice [H_2O(11)] and one coordinated [H_2O(9)] water molecules, forming a 1D single-stranded supramolecular helix. The twofold helix, with a pitch of 17.2093 Å (equal to the length of unit cell *b*), is symmetry-related by a 2_1 screw axis [Fig. S11(a), ESI†]. In accordance with that on the direction of *a*-axis, the absolute helicity of the helix is also left-handed, even though its formation is driven by hydrogen bonds rather than coordination bonds. It is not contradictory to the principle that absolute helicity (based on L-amino acid derivatives) exclusively driven by hydrogen bonds prefers right-handedness whilst coordination bonds (between L-amino acid ligands and metal ions) favor left-handedness, because coordination bonds are stronger than hydrogen bonds. In other words, the absolute helicity on *b*-axis can be seen as a continuation of that on *a*-axis since both of them are determined exclusively by the chirality of the bridging L-Hcala$^-$ ligand. A similar phenomenon was also observed in a reported L-amino acid derivative complex $[ZnL(H_2O)_2]_n \cdot n(H_2O)$ [H_2L = *N*-(4-pyridylmethyl)-L-aspartic acid].[12b] On the direction of *c*-axis, the terminal L-Hcala$^-$ ligand is stretched by hydrogen bonds involving the lattice [H_2O(11)] and the other coordinated [H_2O(10)] water molecules in a head-to-tail way, generating a 1D single-stranded supramolecular helix. It is also a twofold helix with a 2_1 screw axis and a pitch of 23.5764 Å (equal to the length of unit cell *c*) [Fig. S11(b), ESI†]. However, the absolute helicity of this helix, which is merely decided by the chirality of the terminal L-Hcala$^-$ ligand, is right-handed, very similar to the situation in **1L**. Therefore, the final structure of **3L** is a 3D supramolecular framework with M_a–M_b–P_c absolute helicities on the directions of the *a*, *b* and *c*-axes, respectively. The 3D supramolecular structure of **3L** is presented in Fig. S12 (ESI†). The conformation relating to C(8) and N(1) in the bridging ligand and C(19) and N(2) in the terminal ligand adopted the more stable staggered-form, different from those observed in **1L** and **2L** (Fig. S4, ESI†).

The enantiomorph of 2_1 screw axis is itself. Consequently, it is expected that **3D** is also crystallized in the $P2_12_12_1$ space group and have the same crystal structure as that of **3L**, even if we do not get its single crystal structure due to the inferior quality of **3D** crystals (the needle crystals are too small to collect diffraction data). This is further supported by the fact that **3L** and **3D** have the same as-synthesized powder XRD patterns [Fig. S5(b), ESI†]. It is evident that **3D** should have just the opposite $R_{C(10)}$, $R_{C(21)}$ absolute configurations and P_a–P_b–M_c absolute helicities, which is confirmed by CD spectra. A simulated comparison of the absolute helicities of **3L** and **3D**

on the directions of *a*, *b* and *c*-axes is displayed in Fig. S13 (ESI†).

IR spectroscopy and thermogravimetric analysis

1L and **1D**, **2L** and **2D**, **3L** and **3D** have very similar IR spectra, respectively (Fig. S1, ESI†). In the IR spectra of **1L** and **1D**, the broad absorption band in the region 2450–2700 cm^{-1} is due to the stretching vibration of NH_2^+ group.[27] A similar absorption was also observed in a comparable *N*-(2-pyridylmethyl)-L-alanine zwitterion.[11] The strong absorption peak at 1705 cm^{-1} is attributed to the asymmetric stretching vibration (ν_{as}) of the protonated carboxyl group. The ν_{as} of the deprotonated carboxyl group occurs at 1615 cm^{-1}, showing a 90 cm^{-1} red-shift as compared to that of the protonated carboxyl group. These indicate the zwitterionic state of H_2cala molecule, which is consistent with the result of X-ray single crystal structure analysis. The broad band centered at 3414 cm^{-1} is ascribed to the stretching vibration of hydrogen-bonded OH groups. As a comparison, the characteristic absorption peaks of NH_2^+ group at 2450–2700 cm^{-1} and protonated carboxyl group at 1705 cm^{-1} do not appear in the IR spectra of **2L** and **2D**. The peaks at 1610 cm^{-1} and 1375 cm^{-1} are attributed to the ν_{as} and ν_s (symmetric stretching vibration) of monodentate carboxyl groups of the $cala^{2-}$ ligand, respectively. The broad band centered at 3501 cm^{-1} is due to the stretching vibration of hydrogen-bonded water molecules. In the IR spectra of **3L** and **3D**, the typical absorption band of NH_2^+ group at 2450–2700 cm^{-1} is also observed. However, the ν_{as} of protonated carboxyl group does not exist, which suggests the zwitterionic states of $Hcala^-$ ligands, in accordance with the result of X-ray single crystal structure analysis. The peaks at 1600 cm^{-1} and 1396 cm^{-1} are ascribed to the ν_{as} and ν_s of deprotonated carboxyl groups of $Hcala^-$ ligands, respectively. Similar to those in **2L** and **2D**, the broad band centered at 3434 cm^{-1} is also attributed to the stretching vibration of hydrogen-bonded water molecules.

The thermal stability of coordination polymers **2L**, **2D**, **3L** and **3D** were examined by thermogravimetric analysis (TGA) in a nitrogen atmosphere from 40 to 900 °C (Fig. S14, ESI†). **2L** and **2D**, **3L** and **3D** show similar thermal decomposition behaviors respectively, so **2L** and **3L** are described here as representatives. The TGA curve of **2L** undergoes two main stages of weight loss. The weight loss from 40 to 70 °C is observed to be 5.58%, corresponding to the release of the lattice water molecule (theoretical value 5.61%). Then the curve shows a plateau in the temperature range of 70–180 °C. Upon further heating, the weight losses are due to the decomposition of organic ligand and collapse of the 1D coordination polymer. **3L** also undergoes two main steps of weight loss. The lattice and two coordinated water molecules are gradually lost in the temperature range of 40–180 °C (theoretical/found: 8.84%/8.80%). The second step of weight loss occurs after 235 °C, which is attributed to the decomposition of organic ligand and collapse of the 1D coordination polymer.

Chiroptical and photoluminescent properties

In the CD spectra covering the ultraviolet region 200–400 nm [Fig. 9(a)], **1L** and **1D** demonstrate opposite Cotton effects at

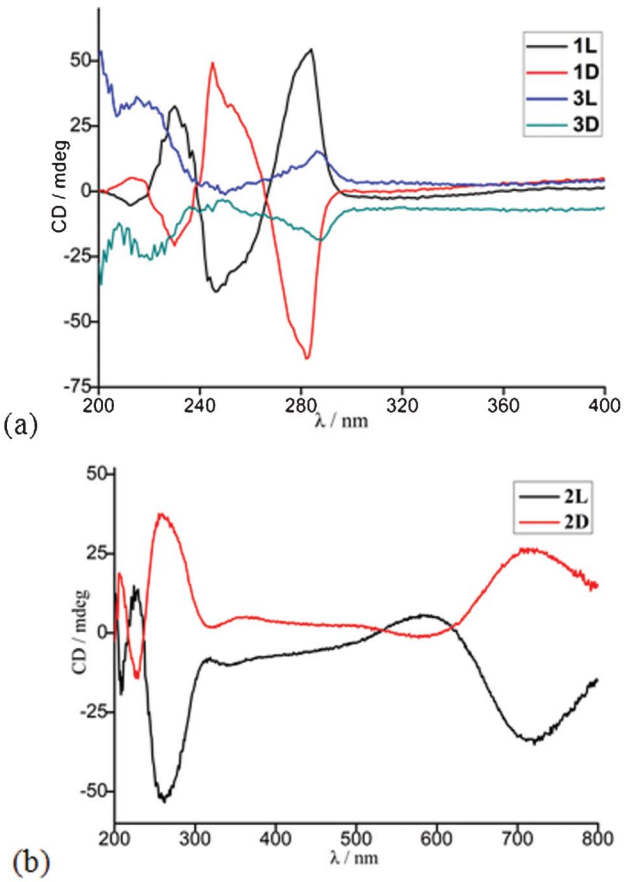

Fig. 9 Solid-state CD spectra of (a): **1L**, **1D**, **3L** and **3D**; (b) **2L** and **2D**.

the same wavelengths (a weak peak at 211 nm, a medium peak at 230 nm, and two strong peaks at 245 and 282 nm) with almost equal intensities, suggesting they are one pair of enantiomers. Similarly, the spectra patterns of **3L** and **3D** are inverted from one another with a strong and broad band centered at 216 nm and a medium band at 287 nm. As compared to the free ligands (**1L** and **1D**), the CD signals of the Cd^{2+} complexes (**3L** and **3D**) in the range of 265–400 nm show 5 nm red-shift (282 → 287 nm), while the Cotton effects from 200 to 265 nm are significantly different. It corresponds to the results of single crystal structure analysis that the free ligands exhibit absolute helicity only on the direction of *b*-axis, while the Cd^{2+} complexes show absolute helicities on three directions parallel to the *a*, *b* and *c*-axes.

In the ultraviolet and visible regions 200–800 nm [Fig. 9(b)], the spectra patterns of **2L** and **2D** are also inverted from each other with two medium peaks at 206 and 225 nm, a strong peak at 259 nm, a weak and broad band centered at 585 nm, and a strong and broad band centered at 717 nm. By comparison with the free ligands, the CD signals of the Cu(II) complexes in the range of 200–235 nm exhibit 5 nm blue-shift (211 → 206 nm and 230 → 225 nm), but the Cotton effects from 235 to 400 nm are distinct. It means that the two new chiral centers [N(1) and Cu(1)] that arise from the stereoselective assembly of ligands and Cu^{2+} ion may exhibit chiral vicinal effects on the phenyl and carboxyl chromo-

phores. More interestingly, Cu^{2+}-based d → d electronic transitions in the visible region are also observed (585 and 717 nm), further proving that the chiralities of the divalent Cu^{2+} centers in **2L** and **2D** are opposite.

Besides, the photoluminescent properties of **1L** and **3L** were examined in the solid-state at room temperature. Upon excitation at 310 and 320 nm, **1L** and **3L** exhibit broad emission bands centered at 361 nm and 368 nm, respectively (Fig. S15, ESI†). Both of them can be assigned to ligand centered fluorescence.

Conclusions

In conclusion, three pairs of enantiomeric coordination helices and supramolecular helices based on *N*-(4-carboxylbenzyl)-L(or D)-alanine ligands were synthesized and characterized. The absolute helicities of **1L** and **1D** controlled by the chirality on the α-C are similar to the situation of α-helices in natural proteins, where L-amino acids result in *P*-helices. The chiralities and absolute helicities of **2L** and **2D** are dependent on the chirality of the ligands, indicating the self-assembly process is highly stereoselective. **3L** and **3D** show ligand-controlled M_a–M_b–P_c and P_a–P_b–M_c helicities on the directions of the *a*, *b* and *c*-axes, respectively. Therefore, the chirality transfer from ligand to complex and crystal exhibited here is efficient. This work provides new perspectives on the rational design of models for researching the relationship between molecular chirality and supramolecular absolute helicity in biopolymers.

Acknowledgements

This work was financially supported by The Science and Technology Department of Guizhou Province (J-LKZS[2012]29) and (J[2010]2121).

Notes and references

1 (*a*) S. F. Mason, *Molecular Optical Activity and the Chiral Discriminations*, Cambridge University Press, Cambridge, 1982; (*b*) J. Zhang and X. H. Bu, *Chem. Commun.*, 2009, 206.
2 D. Voet, J. G. Voet and C. W. Pratt, *Fundamentals of Biochemistry*, John Wiley & Sons Inc., 1999.
3 W. A. Bonner, *Origins Life Evol. Biosphere*, 1994, **24**, 63.
4 T. U. Devi, N. Lawrence, R. R. Babu, S. Selvanayagam, H. Stoeckli-Evans and K. Ramamurthi, *Cryst. Growth Des.*, 2009, **9**, 1370.
5 F. P. Huang, H. Y. Li, J. L. Tian, W. Gu, Y. M. Jiang, S. P. Yan and D. Z. Lian, *Cryst. Growth Des.*, 2009, **9**, 3191.
6 Y. X. Tan, Y. P. He and J. Zhang, *Inorg. Chem.*, 2011, **50**, 11527.
7 J. H. He, G. J. Zhang, D. R. Xiao, H. Y. Chen, S. W. Yan, X. Wang, J. Yang and E. B. Wang, *CrystEngComm*, 2012, **14**, 3609.
8 L. J. Dong, W. Chu, Q. L. Zhu and R. D. Huang, *Cryst. Growth Des.*, 2011, **11**, 93.
9 A. C. Kathalikkattil, P. S. Subramanian and E. Suresh, *Inorg. Chim. Acta*, 2011, **365**, 363.
10 A. C. Kathalikkattil, K. K. Bisht, N. Aliaga-Alcalde and E. Suresh, *Cryst. Growth Des.*, 2011, **11**, 1631.
11 X. F. Li, T. F. Liu, B. Hu, G. L. Li, H. Zhang and R. Cao, *Cryst. Growth Des.*, 2010, **10**, 3051.
12 (*a*) X. L. Yang, M. H. Xie, C. Zou and C. D. Wu, *CrystEngComm*, 2011, **13**, 6422; (*b*) X. L. Yang, M. H. Xie, C. Zou, F. F. Sun and C. D. Wu, *CrystEngComm*, 2011, **13**, 1570.
13 (*a*) B. Sreenivasulu and J. J. Vittal, *Angew. Chem., Int. Ed.*, 2004, **43**, 5769; (*b*) X. B. Wang and J. J. Vittal, *Inorg. Chem.*, 2003, **42**, 5135; (*c*) C. T. Yang, B. Moubaraki, K. S. Murray and J. J. Vittal, *Dalton Trans.*, 2003, 880; (*d*) J. J. Vittal, X. B. Wang and J. D. Ranford, *Inorg. Chem.*, 2003, **42**, 3390.
14 S. P. Wu and C. H. Lee, *CrystEngComm*, 2009, **11**, 219.
15 X. L. Tang, W. H. Wang, W. Dou, J. Jiang, W. S. Liu, W. W. Qin, G. L. Zhang, H. R. Zhang, K. B. Yu and L. M. Zheng, *Angew. Chem., Int. Ed.*, 2009, **48**, 3499.
16 H. Y. Lee, J. Park, M. S. Lah and J. I. Hong, *Cryst. Growth Des.*, 2008, **8**, 587.
17 Z. L. Chen, Y. Su, W. Xiong, L. X. Wang, F. P. Liang and M. Shao, *CrystEngComm*, 2009, **11**, 318.
18 (*a*) J. D. Ranford, J. J. Vittal, D. Q. Wu and X. D. Yang, *Angew. Chem., Int. Ed.*, 1999, **38**, 3498; (*b*) X. B. Wang and J. J. Vittal, *Inorg. Chem. Commun.*, 2003, **6**, 1074; (*c*) C. T. Yang, M. Vetrichelvan, X. D. Yang, B. Moubaraki, K. S. Murray and J. J. Vittal, *Dalton Trans.*, 2004, 113.
19 H. T. Zhang, Y. Z. Li, T. W. Wang, E. N. Nfor, H. Q. Wang and X. Z. You, *Eur. J. Inorg. Chem.*, 2006, 3532.
20 Q. Yue, J. Yang, G. D. Li and J. S. Chen, *Inorg. Chem.*, 2006, **45**, 4431.
21 S. M. Ying, *Inorg. Chem. Commun.*, 2012, **22**, 82.
22 (*a*) G. M. Sheldrick, SHELXS-97, *Program for Solution of Crystal Structures*, University of Göttingen, Germany, 1997; (*b*) G. M. Sheldrick, SHELXL-97, *Program for Refinement of Crystal Structures*, University of Göttingen, Germany, 1997.
23 A. L. Spek, *J. Appl. Crystallogr.*, 2003, **36**, 7.
24 (*a*) H. D. Flack and G. Bernardinelli, *J. Appl. Crystallogr.*, 2000, **33**, 1143; (*b*) A. L. Spek, *Acta Crystallogr., Sect. A: Found. Crystallogr.*, 1990, **46**, C34.
25 H. D. Flack, *Helv. Chim. Acta*, 2003, **86**, 905.
26 H. Zhang, *Coordination Chemistry—Principles and Applications*, Chemical Industry Press, Beijing, 2010.
27 Y. X. Zhao and X. Y. Sun, *Spectroscopic Analysis of Organic Molecular Structure*, Science Press, Beijing, 2003.

